https://doi.org/10.5194/amt-2020-116
Preprint. Discussion started: 26 May 2020

Atmospheric Measurement Techniques Discussions

Methane emissions from an oil sands tailings pond: A quantitative comparison of fluxes derived by different methods

Yuan You[1, §], Ralf M. Staebler[1], Samar G. Moussa[1], James Beck[2], Richard L. Mittermeier[1]

[1]Air Quality Research Division, Environment and Climate Change Canada (ECCC), Toronto, M3H 5T4, Canada
[2]Suncor Energy Inc., Calgary, T2P 3Y7, Canada
[§]Now at Department of Physics, University of Toronto, Toronto, M5S 1A7, Canada

Correspondence: Ralf M. Staebler (ralf.staebler@canada.ca)

Abstract. Tailings ponds in the Alberta Oil Sands Region are significant sources of fugitive emissions of methane to the atmosphere, but detailed knowledge on spatial and temporal variabilities is lacking due to limitations of the methods deployed under current regulatory compliance monitoring programs. To develop more robust and representative methods for quantifying these emissions, three micrometeorological flux methods were applied along with traditional flux chambers to determine fluxes over a 5-week period. Eddy covariance flux measurements provided the benchmark. A method is presented to directly calculate stability-corrected eddy diffusivities that can be applied to vertical gas profiles for gradient flux estimation. Gradient fluxes were shown to agree with eddy covariance within 7%, and inverse dispersion model fluxes within 11%, with an overall uncertainty of 28% for the calculated mean flux. Fluxes were shown to have only a minor diurnal cycle (18% variability) and to be mostly independent of wind speed, air and water surface temperatures. Flux chambers underestimated the fluxes by a factor of 2 in this particular campaign. These measurements indicate that the larger footprint of micrometeorological measurements results in more robust emission estimates representing the whole pond.

1 Introduction

Fossil fuel deposits in the Alberta Oil Sands Region (AOSR) consist of a mixture of quartz sands, slit, clay, bitumen, organics, trace metals, minerals, trapped gases, and pore water (Small et al., 2015). Surface mining is widely practised to extract the oil sands where the deposits are shallow. Extraction of the bitumen from the Oil Sands involves large amounts of warm water, various additives such as caustic soda and sodium citrate, and diluents, such as naphtha or paraffin (Simpson et al., 2010; Small et al., 2015). Non-recovered diluents, additives, and bitumen, along with water end up in large engineered tailings ponds.

There have been a number of studies to quantify the emissions of pollutants to the atmosphere from the various industrial activities associated with the Oil Sands (Simpson et al., 2010; Liggio et al., 2016; Li et al., 2017; Liggio et al., 2017; Baray et al., 2018; Liggio et al., 2019). Pollutant emissions that have been observed from tailings ponds include greenhouse gases (GHGs, mainly methane (CH_4) and carbon dioxide (CO_2)), reduced sulphur compounds, volatile organic compounds (VOCs), and polycyclic aromatic hydrocarbons (PAHs) (Siddique et al., 2007; Simpson et al., 2010; Yeh et al., 2010; Siddique et al., 2011; Siddique et al., 2012; Galarneau et al. 2014; Small et al., 2015; Bari and Kindzierski, 2018; Zhang et al.,2019). However, published studies on atmospheric emissions from tailings

https://doi.org/10.5194/amt-2020-116
Preprint. Discussion started: 26 May 2020

Atmospheric Measurement Techniques Discussions

ponds have been rare (Galarneau et al., 2014; Small et al. 2015; Zhang et al. 2019), and significant gaps remain regarding their contribution to total emission from oil sands operations (Small et al., 2015).

Quantifying greenhouse gases emissions from tailings pond is essential, since facilities are required to report specified gas emissions (Government of Alberta, 2019) and to follow emission standards (Statutes of Alberta, 2016). CH_4 is long-lived in the atmosphere and has a greenhouse gas warming potential per molecule that is 28 times that of CO_2 on a 100-year time horizon, contributing 0.97 W m^{-2} radiative forcing to the total of 2.83 W m^{-2} by all well-mixed greenhouse gases since the beginning of the industrial era (Myhre et al., 2013). CH_4 can be produced by microbes in the oil sands tailings through methanogenic degradation of hydrocarbon in diluents and unrecovered bitumen (Siddique et al., 2007; Penner and Foght, 2010; Siddique et al., 2011; Siddique et al., 2012; Foght et al., 2017; Kong et al., 2019).

Most commonly, flux chambers have been used to determine emission rate of GHGs from tailings ponds (Small et al., 2015; Stantec, 2016). These chambers cover an area of less than 1 m^2 each and result in only short snapshots of emissions that may not capture the spatiotemporal variability of emissions. Tailings ponds in the oil sands region typically have a size of 0.1-10 km^2 with heterogeneous surfaces. Micrometeorological methods of determining fluxes, such as eddy covariance (Foken et al., 2012) and gradient fluxes (Meyers et al., 1996), are non-intrusive and continuous methods that can be used to measure fluxes from area sources. These methods intrinsically produce integrated flux estimates representative of hectares to km^2. In addition, inverse dispersion models (IDMs) (Flesch et al., 1995) and vertical radial plume mapping (VRPM) (Hashmonay et al., 2001) can be used to combine micrometeorological information with measured pollutant concentrations to deduce emission fluxes.

Micrometeorological methods applied to large areas of a tailings pond can provide much needed information on the spatial and temporal variabilities of emission fluxes from tailings ponds as an input for air quality and climate change modelling. Tailings ponds represent a useful testing ground for a multi-method comparison of flux measurement techniques due to their reliability as sources of significant fluxes that are relatively well-defined spatially. This manuscript describes the results of a study comparing flux chambers, eddy covariance, gradient and IDM approaches for estimating emission rates, using a variety of instruments.

2 Field Study

The main site of this study was on the south shore of Suncor Pond 2/3 (Fig. 1; 56°59'0.90"N, 111°30'30.30"W, 305m ASL). The pond liquid surface area was about 2.5 km by 1.3 km. Within 2 km to the south of our measurement site, the landscape included natural landscapes, trees, a workers camp, and parking lots. There were also other facilities and sources around the pond, but too far from our measurement site to contribute to the fluxes measured using the methods in this study (Section 4.2). Measurements were conducted from July 28 to September 5, 2017. The sampling platform was a 32 m mobile tower instrumented at three levels (8m, 18m, and 32m) above ground, plus another sampling level at 4 m above ground on the roof of the trailer housing the instruments. This setup allowed the measurement of the vertical gradient of gaseous pollutants concentrations and meteorological conditions. Gas inlets at these levels were connected to a range of instruments in the trailer located right beside the flux tower, through 45 m of ½" (1.27 cm) Teflon tubing for the upper three levels and 7 m of tubing for the lowest level. A cavity ring-down

https://doi.org/10.5194/amt-2020-116
Preprint. Discussion started: 26 May 2020

Atmospheric Measurement Techniques Discussions

spectroscopy (CRDS) instrument (Picarro, Model G2311f) was used to measure the mole fraction of CH_4, CO_2 and H_2O at 10Hz. It sampled from the 18m level through a 40 m 3/8" Teflon tube at a flow rate of 7 L min^{-1}, ensuring turbulent plug flow. A cavity ring-down spectroscopy instrument (Picarro, Model G2204) was used to measure CH_4 and hydrogen sulfide (H_2S) at three levels, and a CRDS instrument (Picarro, Model G2401-M) was used to measure CH_4, CO_2, CO and H_2O at four levels by cycling through the levels every 10 minutes (i.e. 2.5 minutes at each level). Calibrations of CH_4 for all the CRDS instruments were performed before and after the field project against secondary standards traceable to standards used by Environment and Climate Change Canada (ECCC) for their GHG Observational Program, which are in turn traceable to World Meteorological Organization (WMO) standards.

At each of the three levels on the tower, an ultrasonic anemometer (Campbell Scientific, Model CSAT3) measured the turbulent motions in the atmosphere, i.e. u, v, w (the three orthogonal components of the wind) and T (sonic temperature), at 10Hz. The momentum flux and the sensible heat flux can be calculated from the covariance of the vertical wind component with horizontal wind and temperature fluctuations respectively through eddy covariance. Friction velocity (u_*) can also be calculated from measured u, v, and w. The two lower ultrasonic anemometers pointed towards true north, whereas the ultrasonic anemometer at 32 m pointed at 3.5°. An adjustment to the true north was applied during analysis. There was also a propeller anemometer (Campbell, Model 05103-10) on the trailer roof 4 m above ground, measuring wind speed and direction. Ambient temperature and relative humidity (RH) were measured with sensors at three levels on the tower and 1m above ground (Rotronic, Model HC2-S3-L; shield: Campbell Scientific, Model 43502). Ambient pressure was measured with a barometer (RM Young Model 61202). A net radiometer (Kipp & Zonen, Model CNR1) was used to measure solar radiation during the entire project. An infrared remote sensor (Campbell Scientific, Model SI-111) was mounted at 32m on the tower looking down at an angle of 30° below horizontal to measure the temperature at the pond surface. With an angular field of view of 44°, this results in a footprint ranging from 25 m to 228 m from the tower. Given the location of the tower relative to the pond, winds from between 286° and 76° were defined as coming from the pond.

An open-path Fourier transform infrared (OP-FTIR) spectrometer system (Open Path Air Monitoring System (OPS), Bruker) was set up at the site to measure line-integrated mole fractions of CH_4 and other pollutants. The spectrometer was set up in a trailer next to the main tower about 1.7 m above the ground, pointing to three retro-reflectors 200 m to the east. The lowest retro-reflector was on a tripod, and the higher two retro-reflectors were supported by JLG basket lifts, resulting in heights of the three retro-reflectors of approximately 1.7 m, 11 m, and 23 m above ground. The spectrometer automatically cycled through pointing at these three sequentially. Spectra were measured at a resolution of 0.5 cm^{-1} with 250 scans co-added, resulting in roughly one-minute resolution. Other details on the OP-FTIR setup and spectral retrieval analysis can be found in You et al. (2020).

3 Methods for deriving fluxes

3.1 Eddy covariance flux

Eddy covariance (EC) fluxes represent a direct measurement of the turbulent vertical exchange of a substance, and as such usually serves as the benchmark (Foken et al., 2012) to which more indirect methods (such as those described

https://doi.org/10.5194/amt-2020-116
Preprint. Discussion started: 26 May 2020

Atmospheric Measurement Techniques Discussions

below) can be compared (Bolinius et al., 2016; Prajapati and Santos, 2018). Eddy covariance typically requires fast response time measurements (> 5 Hz) (Foken et al., 2012), which in this study limits the method to sensible and latent heat (H_2O) fluxes, momentum, CO_2 and CH_4.

As summarized in Foken et al. (2012), eddy covariance simply calculates the flux by averaging the product of the deviations of the vertical wind component and a mole fraction from the mean. For compound c and vertical wind component w, the flux F_c is thus

$$F_c(EC) = \overline{w'c'} \quad (1)$$

where the mole fraction $c = \bar{c} + c'$, with the overbar denoting the average and the prime a deviation from it, and similarly for w. To capture the full spectrum or relevant eddy sizes, measurements need to typically be done at > 5 Hz (for the smallest eddies), and the average needs to be 15 minutes or more (to capture the largest eddies). To account for "storage", i.e. the vertical build-up or venting of a gas between the source and the measurement level, a storage term is added, so that the total flux is given by

$$F_c = \overline{w'c'} + \int_0^z \frac{\partial c}{\partial t} \partial z \quad (2)$$

In this study, 30-min averages of the EC flux of CH_4 were calculated by combining the 18 m CRDS CH_4 data with the CSAT measurements. The raw data were processed by Eddypro (version 6.0.0, LI-COR Inc.), and major processes included axis rotation, time lag compensation, WPL (Webb-Pearman-Leuning) density correction, and storage term correction (Foken et al., 2012). The EC flux quality flag was in three categories: 0 (best quality), 1 (good quality), and 2 (poor quality) (Mauder et al., 2006). EC fluxes with flag 0 and 1 were included in further analysis.

3.2 Flux vertical gradient method

Gradient flux estimates are based on relationships between the vertical gradient of mole fractions and the associated flux (down the gradient from high to low mole fractions). In the atmosphere, turbulent exchange dominates molecular diffusion by several orders of magnitude under most conditions, and the factor relating the gradient to the flux is a transfer coefficient dependent on the characteristics of turbulence (first–order closure, *K*-theory), called the eddy diffusivity (K_c) (Stull, 2003a). The flux is then given by

$$F_c = -K_c \frac{\partial c}{\partial z} \quad (3)$$

Where F_c is the gradient flux for a pollutant c, and $\frac{\partial c}{\partial z}$ is the vertical mole fraction gradient. Note that in this notation, K_c incorporates any stability corrections required since stability effects on the relationship between vertical mole fraction gradients and turbulent fluxes are already incorporated. Our approach follows the well-established "modified Bowen Ratio" (MBR) method (Meyers et al., 1996; Bolinius et al., 2016). To calculate K_c of CH_4, the measurements of CH_4 EC flux and a gradient of mole fraction are required by Eq. (3). From the measurements at the 18 m, we have a direct EC flux for CH_4. Since the footprint of fluxes derived from mole fraction gradients between 8 m and 32 m is approximately equivalent to the EC footprint at 18 m (see discussion in Section 4.2), this gradient can be combined with the EC flux to calculate K_c by Eq. (3). However, only a fraction of the observations yield well-resolved CH_4

https://doi.org/10.5194/amt-2020-116
Preprint. Discussion started: 26 May 2020

Atmospheric Measurement Techniques Discussions

fluxes and gradients, whereas a continuous time series of K_m, the eddy diffusivity for momentum (wind speed) by Eq. (4) (Stull, 2003a), can be readily established. Therefore, we establish a relationship between K_c and K_m for those periods when this is feasible, and calculate the ratio of these two, which by definition is the so-called "Schmidt Number" in Eq. (5) (Gualtieri et al. 2017),

$$F_m = -K_m \frac{\partial u}{\partial z} \tag{4}$$

$$S_c = \frac{K_m}{K_c} \tag{5}$$

A near-continuous time series of K_c is then calculated from Eq. (5) and applied to the mole fraction gradients for all the gases measured on the gas profile system to calculate fluxes.

To get the Schmidt Number S_c by Eq. (5), two approaches were used: the first approach is with a constant S_c. Measured K_c was binned with and plotted against K_m. The linear regression of binned K_c with K_m bins was performed. The inverse of this slope (Fig. 2), as defined in Eq. (5), is the Schmidt Number. The least-squared fit produces a $S_c = 0.923$, which compares to published values of 0.99 (Gualtieri et al., 2017). Since due to the intermittent nature of CH_4 a measured K_c is only available a fraction of the time, we use the more continuous momentum eddy diffusivity K_m divided by S_c as our K_c.

The second approach is with variable S_c. Gualtieri et al.(2017) reviewed experimental and numerical simulation studies of turbulent Schmidt number in the atmospheric environment, and reported S_c values from 0.1 to 1.3. Flesch et al. (2002) measured turbulent S_c of a pesticide in the atmosphere from soil emissions. Reported S_c in that study varied from 0.17 to 1.34 and showed that this was not solely due to measurement uncertainty. The S_c in this study also varies significantly over time when the wind was from the pond, from 0.04 to 3.26.

To investigate the real variability in S_c, $S_c = K_{m\_measured}/K_{c\_measured}$ was plotted against the stability parameter z/L (Stull, 2003b), where L is the Obukhov length, for periods when the wind was from the pond direction (Fig. 3). Figure 3 shows that S_c becomes small as z/L indicates increasingly unstable turbulent mixing, i.e. an increasing importance of convective (sensible heat driven) turbulence, which is not captured by an uncorrected K_m, vs. mechanical (momentum driven) turbulence. S_c varies significantly with z/L, and is associated with significant noise near neutral stability (z/L close to 0). To avoid introducing large scatter in the S_c correction near neutral stability, S_c is set as 0.923 when z/L is close to 0. To make the correction function continuous, a step-wise definition for S_c is given:

$$S_c = \begin{cases} 0.126 + 7.81 \times 10^{-9} e^{\left(\frac{\frac{z}{L}+19.5}{1.039}\right)}, & \frac{z}{L} < -0.34 \\ 0.923, & \frac{z}{L} \geq -0.34 \end{cases} \tag{6}$$

This S_c of the entire study period and a time series of $K_c = K_m/S_c$ (corresponding to 8m and 32m measurements) were calculated. Then the gradient flux of CH_4 with corrected K_c was calculated by Eq. (3). Negative half-hour CH_4 gradient fluxes have been filtered out when the EC flux was positive during the same half-hour, since they are most likely due to problems such as shifting wind directions, and unsuitable for calculating gradient fluxes. In the Results and Discussion section, gradient fluxes and plots from the variable S_c approach are shown, and results with constant S_c approach are shown in Table S1 for comparison.

https://doi.org/10.5194/amt-2020-116
Preprint. Discussion started: 26 May 2020


Atmospheric Measurement Techniques Discussions

3.3 Inverse dispersion fluxes

Inverse dispersion models (IDMs) can be used to derive emission rates estimates based on line-integrated or point mole fraction measurements downwind of a defined source. Required inputs include the turbulence statistics between the source and point of observation. Unlike the EC and gradient techniques, IDMs also require an estimation of the background mole fraction of the pollutant upwind of the source. The backward Lagrangian Stochastic (bLS) models are a specific subtype of IDMs. WindTrax 2.0 (Thunder Beach Scientific, http://www.thunderbeachscientific.com (Flesch et al., 1995)) based on a bLS model, is used in this study. The emission rate is calculated through:

$$Q = \frac{(C - C_b)}{(\frac{C}{Q})_{sim}} \quad (7)$$

where C is the pollutant concentration at the measurement location, C_b is the background mole fraction of the pollutant, and $(C/Q)_{sim}$ is the simulated ratio of the pollutant mole fraction at the site to the emission rate from the specified source calculated by the bLS model. In this study, the meteorological condition inputs for bLS model are u_* and L taken from the 30-min averaging calculation of ultrasonic anemometer measurements at 8 m, as well as 30-min average wind directions and ambient temperature directly from the propeller and temperature sensor at 4 m. Periods when u_* <0.15 m/s were disregarded (Flesch et al., 2004). CH_4 mole fraction input was taken from the OP-FTIR measurement which was located right beside the flux tower on the east. Emission rates are calculated by IDM only when the wind came from the pond, including the sectors centred at 270° and 90°.

3.4 Flux chamber measurements

Floating flux chamber measurements of CH_4 and CO_2 were conducted at 15 spots, including 4 within 500 m of the tower, from Aug 31 to September 2, 2017, by Barr Engineering Co., using compliance monitoring procedures established with guidance from the *Quantification of Area Fugitive Emissions at Oil Sands* issued by Alberta Environment and Parks (AEP 2014). On-site analysis of GHG was performed using U.S. Environmental Protection Agency (USEPA) flux chambers with real-time GHG analyzers (Los Gatos Research, Inc., USA). These flux chamber measurements were conducted during daytime with sample durations ranging from 74 to 116 minutes, most of which was for the stabilization of the gas flow inside the flux chamber (i.e. to reach an equilibrium between the flow of the inert carrier gas and the methane evolving from the pond surface). GHG gases reported include CH_4, CO_2 and N_2O.

3.5 Area weight-average of flux

To derive fluxes representing the whole pond, the half-hour fluxes are binned by wind direction into 16 sectors. Area weighted averages of fluxes for the pond F_{pond} are then calculated by

$$F_{pond} = \frac{\sum_{sectors} \overline{F(flux,sector)} * Area(sector)}{\sum_{sectors} Area(sector)} \quad (10)$$

https://doi.org/10.5194/amt-2020-116
Preprint. Discussion started: 26 May 2020


Atmospheric Measurement Techniques Discussions

4 Results and Discussion

4.1 Meteorological conditions

Given the setup of this study at this pond (Fig. 1), the wind came from the north (wind direction (WD) ≥ 286° or WD ≤ 76°) was considered as wind from the pond direction. As shown in the wind rose (Fig. S1), wind coming from the pond occurred only about 22% of the entire measurement period. The dominance of winds from the background directions was known before the study, based on records from monitoring stations in the area, but logistical and access constraints limited us to using the south shore for the setup. There was no significant diurnal variation in wind direction over the entire period (Fig. S2). The ambient temperature during the measurement period varied from 7.5 to 31.1 °C, with an average of 17.5 °C. The mean wind speed measured with the propeller anemometer at 4 m was 3.0 m s^{-1}, with a range from 0 to 14.9 m s^{-1} and quartiles of 1.7 and 4.0 m s^{-1}. The mean friction velocity at 8 m (the lowest height by sonic anemometer measurement) over the whole measurement period was 0.32 m s^{-1}, with a range from 0.03 to 1.01 m s^{-1} and quartiles are 0.20 and 0.42 m s^{-1}. Wind speed and friction velocity had a predictable diurnal pattern, greater during the day than at night (Fig. 4 (a)).

In Fort McMurray during mid-August, the sunrise is near 6:00 MDT (Mountain Daylight Savings Time, UTC-6), solar noon occurs at 13:30 and sunset occurs around 21:00 MDT (Fig. 4 (d)). Winds across the pond and from the south pass over markedly different surface types (liquid pond vs. a mixture of solid surface types), so the sensible heat flux *H* is analyzed separately based on the wind direction (Fig. 4 (e)). During the day (from 8:00 to 19:00), *H* associated with winds across the pond was consistently smaller than *H* with winds from other directions, suggesting the pond absorbs significant solar energy at the site during the day. It is also worth mentioning that *H* stayed positive during the night when the wind came across the pond, consistent with the observation that the pond surface temperature was greater than the air temperature (Fig. 4 (b,c)). These resulted in convective turbulent transport of species from the pond surface throughout the night.

4.2 Footprint of flux measurements

The footprint of a micrometeorological flux measurement, i.e. the area upwind that contributes to the flux at the point of observation, depends on the wind speed and the dynamic stability of the surface layer. The footprints of EC fluxes measured at 18m at each half-hour period were estimated using the algorithm by Kljun et al. (2015), which takes mean wind speed, boundary layer height, wind direction, friction velocity, Obukhov length, and standard deviation of wind speed. Boundary layer height was estimated using the LIDAR measurements at Fort McKay in August 2013 (Strawbridge et al., 2018). An example of the footprint is shown in Fig. S3 (a), and footprints over the entire measurement period are summarized in the rose plot in Fig. S3 (b) showing the EC flux footprint lies mostly within the edges of the pond under most conditions.

For flux gradient measurements, the effective footprint is the same as the EC footprint at the geometric mean of the two sample heights (Horst, 1999), for a homogeneous surface area upwind. In this study, gradients between 8 m and 32 m therefore have a footprint equivalent to that for EC at 16 m, reasonably close to where the 18 m EC fluxes were measured. Since the concentration footprint at the upper (32 m) level is however larger than the concentration footprint at the lower (8 m) level, the gradient flux may be affected by sources beyond the geometric mean footprint.

https://doi.org/10.5194/amt-2020-116
Preprint. Discussion started: 26 May 2020


Atmospheric Measurement Techniques Discussions

4.3 Eddy covariance flux

Analysis of CH_4 mole fractions at 18 m as shown in Fig. 5 clearly indicates that CH_4 was elevated when the wind was from the pond direction, and it was steady at round 1.9 ppm when the wind was from other directions (Fig. 5 and 6). Besides sectors from the pond directions, Fig. 7 shows CH_4 fluxes significantly larger than zero from two sectors centred with 270° and 90°. These two sectors cover the boundaries of pond and non-pond areas. Therefore, measured results for air coming from these two sectors could represent a mixture of air carrying pond emissions and air from the southwest close to the pond shoreline. EC fluxes from the four wind directions sectors centred in the range of 292.5° to 0° are close to each other.

There was no discernible diurnal pattern of the CH_4 EC flux when the wind came from the pond direction (WD ≥ 286°, or WD ≤ 76°) (relative standard deviation is 18%) (Fig. S4 (a)). Diurnal pattern of another three sectors when the wind was not from the pond were studied. The sector 259° ≤ WD < 286° (Fig. S4 (b)) contains a mixture of pond emission and the shore of pond, and it also showed no significant diurnal pattern. The sector 214° ≤ WD < 259° (Fig.S4 (c) mainly covers trees and a lake, and showed a slightly increased flux during 12:00-18:00, which is likely due to biogenic emission from trees and soils (Covey and Megonigal, 2019). The sector 124° ≤ WD < 146° (Fig. S4 (d)) covered a workers' lodge and parking lots, and CH_4 emissions and diurnal variation were close to zero. The lack of a diurnal variation of CH_4 EC flux observed when the wind was from the pond in this study was similar to the diurnal variation of CH_4 EC flux at another tailings pond reported by Zhang et al. (2019).

Relationships between the flux and various meteorological parameters were investigated, and results show that fluxes were independent of wind speed, u_*, water surface temperature, or the temperature difference between the water surface and 8 m (Fig. S5), i.e. they were not drivers of the CH_4 emission rate. CH_4 at this site is mainly produced through the methanogenesis of hydrocarbon by the microbes in the fine tailings covering a range of depth in the pond (Penner and Foght, 2010; Siddique et al., 2011;Siddique et al., 2012), and therefore is not affected much by the meteorological conditions at the surface or above the pond.

4.4 CH_4 gradient flux and comparison with EC flux

The CH_4 mole fraction measured at 8 m and 32 m show that winds across the pond carried significantly more CH_4 than from other directions, and there was a clear vertical gradient with mole fraction at 8 m on the order of 0.5 ppm or more higher than at 32 m (Fig. 6). The gradient flux derived from measurements at 8m and 32m shows that the flux was minimal when the wind was from other directions, similar to the EC flux (Fig. S6). The average CH_4 gradient flux was 7% less than the EC flux (Table 1), and CH_4 gradient flux agreed well with EC flux (slope=1.03, r^2=0.65) (Fig. 8).

Studies comparing MBR and eddy covariance CH_4 fluxes are rare. Zhao et al. (2019) compared CH_4 fluxes from an MBR method as well as from an aerodynamic flux model to EC fluxes for two small fish ponds, and showed that the MBR fluxes were well correlated with EC fluxes, with a mean 27% greater than the EC mean flux. The gradient flux calculation in our study can be considered a hybrid of the MBR and aerodynamic methods, based on a continuous time series of eddy diffusivities for momentum, scaled by the eddy diffusivity for CH_4. The gradient fluxes of CH_4 agree well with EC flux in our study, indicating that the derived eddy diffusivity K_c for CH_4 can be utilized for other

https://doi.org/10.5194/amt-2020-116
Preprint. Discussion started: 26 May 2020

Atmospheric Measurement Techniques Discussions

gaseous pollutants when the wind was from the pond direction (Meyers et al., 1996). Gradient fluxes of VOCs and reduced sulfur components from the pond are discussed in Moussa et al. (2020a) and Moussa et al. (2020b). Other studies comparing MBR with eddy covariance methods on other gases fluxes, such as CO_2, have been reported. Xiao et al. (2014) showed that fluxes of CO_2 from these two methods were comparable at Lake Taihu. Wolf et al. (2008) and Bolinius et al. (2016) used eddy diffusivity of heat to derive gradient fluxes of CO_2 over trees, and showed they were comparable with EC fluxes.

Gradient fluxes were also calculated with the constant S_c approach, as described in Section 3.2, and results are listed in Table S1. Gradient flux calculated from a constant S_c were lower than gradient fluxes with the variable S_c approach. Results from this study clearly present the variable nature of S_c, and that correcting S_c with stability z/L is effective to improve gradient flux calculations. After correcting S_c, CH_4 gradient fluxes compared well with EC flux.

4.5 CH_4 inverse dispersion flux and comparison with EC flux

Compared to point measurements, path-integrated measurements have the advantage of being less sensitive to changes of wind direction and being representative of larger areal averages (Flesch et al. 2004). Therefore, the bottom path-integrated CH_4 mole fraction of the FTIR was used as input for IDM flux estimate. The bottom path measurement had the greatest signal-to-noise ratio, and a footprint of on the order of 1-2 km, which is comparable to the footprint of the EC and gradient fluxes (Fig. S3). CH_4 IDM flux based on path-integrated mole fraction inputs from OP-FTIR bottom path measurements compared well to EC flux. IDM and EC flux showed reasonable correlation (r^2=0.46) with a slope of 0.93 (Fig. 9). The interquartile ranges of the fluxes from these two methods overlap. The average of IDM flux was 11% smaller than EC flux. Consistent with EC flux, IDM flux also showed minimal diurnal variations when the wind came from the pond directions (Fig. S7), with smaller fluxes from 8:00 to 20:00. Some of the differences are likely due to the different footprints of the two measurements. The footprint for turbulent fluxes is smaller than the footprint for concentrations at the same height (Schmid, 1994).

Since the background mole fraction input for IDM calculation could affect the flux estimates, two approaches of determing backgound mole fraction of CH_4 for model inputs were tested: the daily minimum of CH_4 from wind sectors between 180° and 240° of OP-FTIR at our site; the CH_4 from another independent OP-FTIR measurement on the north shore of this pond (details are described in You et al. (2020)). Results IDM fluxes with these two background approaches agreed well (You et al. 2020).

4.6 Flux chamber measurements

Fluxes from the 15 measurements over 3 days in the bubbling zones varied from 0.9 to 5.1 g m^{-2} d^{-1}, with an average of 2.8 g m^{-2} d^{-1}. The average flux of the five measurements on the last day Sept 2 is 3.6 g m^{-2} d^{-1}, which is the highest amongst the 3 days. The great variation amongst these 15 measurements show the pond was highly heterogeneous in terms of CH_4 emissions. The average fluxes from these flux chamber measurements are about half of average fluxes from EC, gradient, and IDM methods. While the flux chamber measurements were deployed over the three days, the wind was from the south, so no simultaneous comparison could be made between flux chamber measurements and micrometeorological methods. However, based on the micrometeorological fluxes spanning more than a month, there

https://doi.org/10.5194/amt-2020-116
Preprint. Discussion started: 26 May 2020


Atmospheric Measurement Techniques Discussions

is no evidence of day-to-day variability of this magnitude, and we conclude that the mismatch is due to spatial or methodological differences.

Annual compliance flux chamber measurements in 2016 resulted in pond average fluxes of 5.3 g m^{-2} d^{-1}, and 11.1 g m^{-2} d^{-1} in 2018, despite similar operational parameters in these years as in 2017. We conclude that the underestimate in 2017 is not an indication of a systematic bias of flux chambers, but rather a measure of the uncertainty involved in flux estimates based on snapshot chamber measurements.

A few other studies have also discussed differences between flux chambers and micrometeorological methods. Zhang et al. (2019) measured CH_4 emission from another tailings pond, and reported flux chamber measurements were more than 10 times greater than fluxes from EC method. They stated that strong eruptions of bubbles could overwhelm the chamber to result in a local underestimation of the flux. On the other hand, the lower EC flux estimate suggests that the area average flux was being overestimated by extrapolation from the chambers, which may have preferentially been located over bubble zones. Their EC fluxes were two orders of magnitude smaller than CH_4 flux in this study. Results from this study and Zhang et al. (2019) suggest that average tailings pond CH_4 emission extrapolated from a few individual flux chamber measurements may significantly underestimate or overestimate fluxes relative to area-averaging micrometeorological measurements.

This has also been shown over other water surfaces. Podgrajsek et al. (2014) investigated CH_4 fluxes at the lake Tamnaren, and reported the fluxes from EC and flux chamber were on the same order of magnitude. They stated due to the non-continuous measurement of flux chambers, some high flux short episodes could be missed. Schubert et al. (2012) measured CH_4 fluxes from Lake Rotsee, and reported the fluxes from EC and flux chamber compared well. Erkkilä et al. (2018) measured CH_4 flux at Lake Kuivajärvi with the two methods when the lake was stratified, and reported flux chamber measurements were significantly greater than EC fluxes. In conclusion, due to the spatial heterogeneity of fluxes on a scale smaller than the spatially integrating micrometeorological methods, reliance on a limited number of flux chamber measurements can result in significant year-to-year variability.

5 Conclusions and Implications

Results in this study have provided several estimates of the emission of CH_4 from this tailings pond using different micrometeorological methods, for a period of a month. The gradient and inverse dispersion methods agreed well with the more fundamental eddy covariance results (within 7% and 11%), which lends confidence that the former two methods can reliably provide flux estimates for other gases emanating from the pond. These results were also compared to flux chamber measurements at this pond taken during the study, showing flux chamber estimates were 54% lower in 2017.

Emissions reported in Small et al. (2015) and a Stantec report (2016) (Table 2) represent estimates extrapolated from individual flux chamber measurements, and did not incorporate any seasonal variations for microbial CH_4 emissions. Therefore, to compare result of this study to results summarized in Small et al. (2015), we simply used 1 year =365 equal days. Small et al. (2015) showed that CH_4 emissions from the same pond were 2.6 g m^{-2} d^{-1} based on the averaging of flux chamber measurements during August to October in 2010 and 2011. A Stantec compliance report (2016) presented flux chamber measurements on this pond with resulting average fluxes of 12.9 and 2.1 g m^{-2} d^{-1}

https://doi.org/10.5194/amt-2020-116
Preprint. Discussion started: 26 May 2020

Atmospheric Measurement Techniques Discussions

(bubbling and quiescent zones, respectively) in 2013, and 9.6 g m^{-2} d^{-1} and below detection limit respectively in 2014. Eddy covariance fluxes of CH_4 in this study are 120% greater than flux chamber measurements which were taken during the last few days of this project and 134% greater than emissions reported in Small et al. (2015). However, CH_4 fluxes in this study are 36% to 52% smaller than the fluxes from the bubbling zones in 2013 and 2014 (Stantec, 2016). The big differences between flux chamber measurements in the bubbling and quiescent zones may suggest micrometeorological measurements with a bigger footprint will perform better in quantifying emission from the whole pond. It is worth noting that the seasonal variation of fugitive emission from tailings pond is still not well understood, and that different daily emissions are derived from the tabulated annual results from Small et al. (2015) depending on the annual extrapolation model used. This reflects a general complication when comparing the five weeks emission results in this study to annual emissions reported in the past.

Baray et al. (2018) calculated CH_4 emission from this pond based on airborne measurement in 2013 over the whole facility, combined with reported statistics stating that 58% of CH_4 emissions within the facility were from tailings ponds, and 85% of emissions from these tailings ponds were from Pond 2/3. This resulted in an estimate of 2.0 ± 0.3 tonnes h^{-1}, which converts to 17.1 g m^{-2} d^{-1} (for a pond area of 2.8 km^2, Small et al. (2015) Table 2). This emission rate is significantly (180%) greater than emissions from the three micrometeorological methods in this study, possibly because of the uncertainties in the reported percentage contribution of CH_4 emissions from this pond to the whole facility.

Suncor reported facility-wide emissions of CH_4 for 2017 of 5977 tonnes (Government of Canada, 2017). The emissions measured during the 5 weeks of this study extrapolated to the year result in 5121 tonnes, i.e. 86% of this total. This extrapolation assumes seasonal invariance of CH_4 emissions (e.g. January emissions are the same as August emissions) as is common practice in monitoring reports (cf. Stantec, 2016).

When comparing CH_4 emissions in this study to emissions summarized in Table 1, it must be kept in mind that different time periods are being compared, and that several factors may contribute to variability of the emissions (Siddique et al. 2007 and 2012). Pond 2/3 is an active pond, and the amount and characteristics of input streams are variable with time. Some of the facility specific variables which could affect the methane emissions include: the amount of diluent loss to the pond, the proportions of diluent and hydrocarbons in the froth treatment tailings (FTT) that enter matured fine tailings (MFT) layers in the pond, density of microbes in the MFT, physical disturbance of the MFT layers, transferring activities of the MFT, pond water temperature change and consequential density inversion between oil layers and water in the pond, FTT discharge diluent composition change, introduction of new materials and chemicals into the MFT, and consequential change in microbial community (Small et al. 2015; Foght et al. 2017). Another independent approach of estimating CH_4 emissions is using an emission factor (EF) combined with diluent discharge rates to the pond. The EF was based on an MFT characterization and kinetics of methanogenesis for a matured pond. Pond 2/3 is presumably similar in maturity and properties with the studied MFT in other oil sands facility (Siddique et al. 2008). After incorporating the diluent loss to the pond, the daily CH_4 emissions were calculated and integrated into an annual emission of 5860 tonnes for 2017, comparable to annual emissions extrapolated from the micrometeorological methods in this study. This approach requires some assumptions: first, that the kinetics of

https://doi.org/10.5194/amt-2020-116
Preprint. Discussion started: 26 May 2020


Atmospheric Measurement Techniques Discussions

methanogenesis are a function of the maturity of the microbial community within the target MFT; and second, that the properties of the diluent feed stream remain constant over the period considered. This approach can provide emission estimates continually provided that the microbial state in the MFT and the diluent discharge volumes and properties are tracked and remain consistent.

To put the CH_4 emissions into a global warming context, the CH_4 fluxes can be combined with concurrent flux measurements of CO_2 with the same instrumentation. Assuming a global warming potential (GWP) of CH_4 = 28 (Myhre et al., 2013), the equivalent CO_2 flux from this tailings pond $F\_CO_{2eq}=CO_2+ (CH_4\times GWP)$ = 158,666 tonnes $year^{-1}$. This accounts for only 2% of Suncor's facility CO_{2eq} emissions in 2017 due to the dominance of CO_2 emissions.

https://doi.org/10.5194/amt-2020-116
Preprint. Discussion started: 26 May 2020

Atmospheric Measurement Techniques Discussions

Data availability.

All data are publically available at http://data.ec.gc.ca/data/air/monitor/source-emissions-monitoring-oil-sands-region/emissions-from-tailings-ponds-to-the-atmosphere-oil-sands-region/.

Author contribution.

YY and RS conducted the research and wrote the manuscript; SGM contributed flux analysis and editing; RM contributed CH_4 data; JB contributed operational data on the pond and contributed to the writing.

Competing interests.

Dr. Beck is an employee of Suncor Energy. The other authors have no competing interests.

Acknowledgements.

The authors thank the technical team of Andrew Sheppard, Roman Tiuliugenev, Raymon Atienza and Raj Santhaneswaran for their invaluable contributions throughout, Julie Narayan for spatial analysis, Stewart Cober for management and Stoyka Netcheva for home base logistical support. We thank Suncor and its project team (Dan Burt et. al.), AECOM (April Kliachik, Peter Tkalec) and SGS (Nathan Grey, Ardan Ross) for site logistics support. This work was partially funded under the Oil Sands Monitoring Program and is a contribution to the Program but does not necessarily reflect the position of the Program. We also acknowledge funding from the Program for Energy Research and Development (NRCan) and from the Climate Change and Air Quality Program (ECCC).

References

Alberta Energy Regulator, Directive 085, Fluid Tailings Management for Oil Sands Mining Projects. (2017). https://www.aer.ca/documents/directives/Directive085.pdf (last accessed: Oct 21st, 2019)

Alberta Environment and Parks: Quantification of area fugitive emissions at oil sands mines. https://open.alberta.ca/publications/quantification-of-area-fugitive-emissions-at-oil-sands-mines-version-2-0, 2014 (last accessed: Dec 3, 2019).

Bari, M. A., and Kindzierski, W. B.: Ambient volatile organic compounds (VOCs) in communities of the Athabasca oil sands region: Sources and screening health risk assessment, Environ. Pollut., 235, 602-614, http://doi.org/10.1016/j.envpol.2017.12.065, 2018.

Bolinius, D. J., Jahnke, A., and MacLeod, M.: Comparison of eddy covariance and modified Bowen ratio methods for measuring gas fluxes and implications for measuring fluxes of persistent organic pollutants, Atmos. Chem. Phys., 16, 5315-5322, http://doi.org/10.5194/acp-16-5315-2016, 2016.

https://doi.org/10.5194/amt-2020-116
Preprint. Discussion started: 26 May 2020

Atmospheric Measurement Techniques Discussions

Businger, J. A., Wyngaard, J. C., Izumi, Y., and Bradley, E. F.: Flux- profile relationships in the atmospheric surface layer, J. Atmos. Sci., 28, 181-189, 1971.

Covey, K. R., and Megonigal, J. P.: Methane production and emissions in trees and forests, New Phytol., 222, 35-51, http://doi.org/10.1111/nph.15624, 2019.

Dyer, A. J., and Hicks, B. B.: Flux-gradient relationships in the constant flux layer, Quarterly Journal of the Royal Meteorological Society, 96, 715-721, http://doi.org/10.1002/qj.49709641012, 1970.

Erkkilä, K. M., Ojala, A., Bastviken, D., Biermann, T., Heiskanen, J., Lindroth, A., Peltola, O., Rantakari, M., Vesala, T., and Mammarella, I.: Methane and carbon dioxide fluxes over a lake: Comparison between eddy covariance, floating chambers and boundary layer method, Biogeosciences, 15, 429-445, http://doi.org/10.5194/bg-15-429-2018, 2018.

Flesch, T. K., Wilson, J. D., and Yee, E.: Backward-time Lagrangian stochastic dispersion models and their application to estimate gaseous emissions, J. Appl. Meteorol., 34, 1320-1332, 1995.

Flesch, T. K., Prueger, J. H., and Hatfield, J. L.: Turbulent Schmidt number from a tracer experiment, Agric. For. Meterol., 111, 299-307, https://doi.org/10.1016/S0168-1923(02)00025-4, 2002.

Flesch, T. K., Wilson, J. D., Harper, L. A., Crenna, B. P., and Sharpe, R. R.: Deducing ground-to-air emissions from observed trace gas concentrations: A field trial, J. Appl. Meteorol., 43, 487-502, 2004.

Foght, J. M., Gieg, L. M., and Siddique, T.: The microbiology of oil sands tailings: Past, present, future, FEMS Microbiol. Ecol., 93, http://doi.org/10.1093/femsec/fix034, 2017.

Foken, T., Aubinet, M., and Leuning, R.: Eddy Covariance: A practical guide to measurement and data analysis, Eddy covariance method, edited by: Aubinet;, M., Vesala;, T., and Papale., D., Springer, 438 pp., 2012.

Galarneau, E., Hollebone, B. P., Yang, Z., and Schuster, J.: Preliminary measurement-based estimates of PAH emissions from oil sands tailings ponds, Atmos. Environ., 97, 332-335, http://doi.org/10.1016/j.atmosenv.2014.08.038, 2014.

Government of Alberta, Lower Athabasca Region – Tailings management framework for the minable Athabasca Oil Sands. 2015. https://open.alberta.ca/dataset/962bc8f4-3924-46ce-baf8-d6b7a26467ae/resource/7c49eb63-751b-49fd-b746-87d5edee3131/download/2015-larp-tailingsmgtathabascaoilsands.pdf. (last accessed: Oct 21st, 2019)

Government of Alberta, Specified gas reporting standard. 2019 Version 11.0 https://open.alberta.ca/dataset/c5471471-79a3-456b-a183-997692da2576/resource/14073f8c-deab-410e-a9ab-ed326e5e4052/download/specified-gas-reporting-standard-v-11.pdf. (last accessed: Oct 21st, 2019)

Government of Canada Greenhouse Gas Reporting Program, https://climate-change.canada.ca/facility-emissions/GHGRP-G10558-2017.html, 2017. (last accessed: Dec 4th, 2019)

Gualtieri, C., Angeloudis, A., Bombardelli, F., Jha, S., and Stoesser, T.: On the Values for the Turbulent Schmidt Number in Environmental Flows, Fluids, 2, http://doi.org/10.3390/fluids2020017, 2017.

https://doi.org/10.5194/amt-2020-116
Preprint. Discussion started: 26 May 2020

Hashmonay, R. A., Natschke, D. F., Wagoner, K., Harris, D. B., Thompson, E. L., and Yost, M. G.: Field evaluation of a method for estimating gaseous fluxes from area sources using open-path fourier transform infrared, Environ. Sci. Tech., 35, 2309-2313, http://doi.org/10.1021/es0017108, 2001.

Horst, T. W.: The footprint for estimation of atmosphere-surface exchange fluxes by profile techniques, Bound-Lay. Meteorol., 90, 171-188, 1999.

Kljun, N., Calanca, P., Rotach, M. W., and Schmid, H. P.: A simple two-dimensional parameterisation for Flux Footprint Prediction (FFP), Geosci. Model Dev., 8, 3695-3713, http://doi.org/10.5194/gmd-8-3695-2015, 2015.

Kong, J. D., Wang, H., Siddique, T., Foght, J., Semple, K., Burkus, Z., and Lewis, M. A.: Second-generation stoichiometric mathematical model to predict methane emissions from oil sands tailings, Sci. Total Environ., 694, 133645, https://doi.org/10.1016/j.scitotenv.2019.133645, 2019.

Li, S. M., Leithead, A., Moussa, S. G., Liggio, J., Moran, M. D., Wang, D., Hayden, K., Darlington, A., Gordon, M., Staebler, R., Makar, P. A., Stroud, C. A., McLaren, R., Liu, P. S. K., O'Brien, J., Mittermeier, R. L., Zhang, J., Marson, G., Cober, S. G., Wolde, M., and Wentzell, J. J. B.: Differences between measured and reported volatile organic compound emissions from oil sands facilities in Alberta, Canada, Proc. Natl. Acad. Sci. U. S. A., 114, E3756-E3765, http://doi.org/10.1073/pnas.1617862114, 2017.

Liggio, J., Li, S. M., Staebler, R. M., Hayden, K., Darlington, A., Mittermeier, R. L., O'Brien, J., McLaren, R., Wolde, M., Worthy, D., and Vogel, F.: Measured Canadian oil sands CO_2 emissions are higher than estimates made using internationally recommended methods, Nat. Commun., 10, http://doi.org/10.1038/s41467-019-09714-9, 2019.

Liggio, J., Moussa, S. G., Wentzell, J., Darlington, A., Liu, P., Leithead, A., Hayden, K., O'Brien, J., Mittermeier, R. L., Staebler, R., Wolde, M., and Li, S. M.: Understanding the primary emissions and secondary formation of gaseous organic acids in the oil sands region of Alberta, Canada, Atmos. Chem. Phys., 17, 8411-8427, http://doi.org/10.5194/acp-17-8411-2017, 2017.

Mauder, M., Liebethan, C., Göckede, M., Leps, J-P, Beyrich, F., and Foken, T.; Processing and quality control of flux data during LITFASS-2003, Bound-Lay. Meteorol., 121, 67-88, http://doi.org/10.1007/s10546-006-9094-0, 2006.

Meyers, T. P., Hall, M. E., Lindberg, S. E., and Kim, K.: Use of the modified bowen-ratio technique to measure fluxes of trace gases, Atmos. Environ., 30, 3321-3329, https://doi.org/10.1016/1352-2310(96)00082-9, 1996.

Moussa, S.G., Staebler, R.M., You, Y., Leithead, A., Yousif, M.A., Brickell, P., Beck, J. Jiang, Z., Li, S.-M., Liggio, J., Wren, S.N., Darlington, A., and Narayan, J.: Fugitive Emissions of Volatile Organic Compounds from a Tailings Pond in the Oil Sands Region of Alberta. In review, Env. Sci. Tech., 2020a.

Moussa, S.G., Staebler, R.M. You, Y., Leithead, A., Mittermeier, R., Hayden, K., Mihele, C., and Beck, J.: Total Reduced Sulfur Fugitive Emissions from an Oil Sands Tailings Pond: Sources and Estimates. In review, Atmos. Env., 2020b.

https://doi.org/10.5194/amt-2020-116
Preprint. Discussion started: 26 May 2020


Atmospheric Measurement Techniques Discussions

Myhre, G., Shindell, D., Bréon, F.-M., Collins, W., Fuglestvedt, J., Huang, J., Koch, D., Lamarque, J.-F., D. Lee, B. M., Nakajima, T., Robock, A., Stephens, G., Takemura, T., and Zhang, H.: Anthropogenic and Natural Radiative Forcing. In: Climate change 2013: The physical science basis: Working Group I contribution to the fifth assessment report of the Intergovernmental Panel on Climate Change, in, edited by: Stocker, T. F., D. Qin, G.-K. Plattner, M. Tignor, S.K. Allen, J. Boschung, A. Nauels, Y. X., Bex, V., and Midgley, P. M., Cambridge University Press, Cambridge, United Kingdom and New York, NY, USA., Chapter 8, Section 8.7, 659-740, 2013.

Penner, T. J., and Foght, J. M.: Mature fine tailings from oil sands processing harbour diverse methanogenic communities, Can. J. Microbiol., 56, 459-470, http://doi.org/10.1139/W10-029, 2010.

Podgrajsek, E., Sahlée, E., Bastviken, D., Holst, J., Lindroth, A., Tranvik, L., and Rutgersson, A.: Comparison of floating chamber and eddy covariance measurements of lake greenhouse gas fluxes, Biogeosciences, 11, 4225-4233, http://doi.org/10.5194/bg-11-4225-2014, 2014.

Rooney, R. C., Bayley, S. E., and Schindler, D. W.: Oil sands mining and reclamation cause massive loss of peatland and stored carbon, Proc. Natl. Acad. Sci. U. S. A., 109, 4933-4937, http://doi.org/10.1073/pnas.1117693108, 2012.

Prajapati, P., and Santos, E. A.: Comparing methane emissions estimated using a backward-Lagrangian stochastic model and the eddy covariance technique in a beef cattle feedlot, Agric. For. Meterol., 256-257, 482-491, https://doi.org/10.1016/j.agrformet.2018.04.003, 2018.

Salloum, M. J., Dudas, M. J., and Fedorak, P. M.: Microbial reduction of amended sulfate in anaerobic mature fine tailings from oil sand, Waste Manage. Res., 20, 162-171, http://doi.org/10.1177/0734242X0202000208, 2002.

Schmid, H. P.: Source areas for scalars and scalar fluxes, Bound-Lay. Meteorol., 67, 293-318, http://doi.org/10.1007/BF00713146, 1994.

Schubert, C. J., Diem, T., and Eugster, W.: Methane emissions from a small wind shielded lake determined by eddy covariance, flux chambers, anchored funnels, and boundary model calculations: A comparison, Environ. Sci. Tech., 46, 4515-4522, http://doi.org/10.1021/es203465x, 2012.

Siddique, T., Fedorak, P. M., MacKinnon, M. D., and Foght, J. M.: Metabolism of BTEX and Naphtha Compounds to Methane in Oil Sands Tailings, Environmental Science & Technology, 41, 2350-2356, http://doi.org/10.1021/es062852q, 2007.

Siddique, T., Gupta, R., Fedorak, P. M., MacKinnon, M. D., and Foght, J. M.: A first approximation kinetic model to predict methane generation from an oil sands tailings settling basin, Chemosphere, 72, 1573-1580, https://doi.org/10.1016/j.chemosphere.2008.04.036, 2008.

Siddique, T., Penner, T., Semple, K., and Foght, J. M.: Anaerobic biodegradation of longer-chain n-alkanes coupled to methane production in oil sands tailings, Environ. Sci. Tech., 45, 5892-5899, http://doi.org/10.1021/es200649t, 2011.

Siddique, T., Penner, T., Klassen, J., Nesbø, C., and Foght, J. M.: Microbial communities involved in methane production from hydrocarbons in oil sands tailings, Environ. Sci. Tech., 46, 9802-9810, http://doi.org/10.1021/es302202c, 2012.

Simpson, I. J., Blake, N. J., Barletta, B., Diskin, G. S., Fuelberg, H. E., Gorham, K., Huey, L. G., Meinardi, S., Rowland, F. S., Vay, S. A., Weinheimer, A. J., Yang, M., and Blake, D. R.: Characterization of trace gases measured over Alberta oil sands mining operations: 76 speciated C_2–C_{10} volatile organic compounds (VOCs), CO_2, CH_4, CO, NO, NO_2, NO_y, O_3 and SO_2, Atmos. Chem. Phys., 10, 11931-11954, http://doi.org/10.5194/acp-10-11931-2010, 2010.

Small, C. C., Cho, S., Hashisho, Z., and Ulrich, A. C.: Emissions from oil sands tailings ponds: Review of tailings pond parameters and emission estimates, Journal of Petroleum Science and Engineering, 127, 490-501, http://doi.org/10.1016/j.petrol.2014.11.020, 2015.

Stantec: Air pollutant and GHG emissions from mine faces and tailings ponds, 413, 2016.

Statutes of Alberta, Oil sands emissions limit act Chapter O-7.5 (2016). http://www.qp.alberta.ca/documents/Acts/O07p5.pdf. (last accessed: Oct 21st, 2019)

Strawbridge, K. B., Travis, M. S., Firanski, B. J., Brook, J. R., Staebler, R., and Leblanc, T.: A fully autonomous ozone, aerosol and nighttime water vapor lidar: a synergistic approach to profiling the atmosphere in the Canadian oil sands region, Atmos. Meas. Tech., 11, 6735-6759, http://doi.org/10.5194/amt-11-6735-2018, 2018.

Stull, R. B.: Chapter 6.4 Local Closure – First Order, in: An Introduction To Boundary Layer Meteorology, Kluwer Academic Publishers, Netherland, 203-214, 2003a.

Stull, R. B.: Chapter 5 Turbulence Kinetic Energy, Stability and Scaling, in: An Introduction To Boundary Layer Meteorology, Kluwer Academic Publishers, Netherland, 182, 2003b.

Wolf, A., Saliendra, N., Akshalov, K., Johnson, D. A., and Laca, E.: Effects of different eddy covariance correction schemes on energy balance closure and comparisons with the modified Bowen ratio system, Agric. For. Meterol., 148, 942-952, http://doi.org/10.1016/j.agrformet.2008.01.005, 2008.

Xiao, W., Liu, S., Li, H., Xiao, Q., Wang, W., Hu, Z., Hu, C., Gao, Y., Shen, J., Zhao, X., Zhang, M., and Lee, X.: A flux-gradient system for simultaneous measurement of the CH_4, CO_2, and H_2O fluxes at a lake-air interface, Environ. Sci. Tech., 48, 14490-14498, http://doi.org/10.1021/es5033713, 2014.

Yeh, S., Jordaan, S. M., Brandt, A. R., Turetsky, M. R., Spatari, S., and Keith, D. W.: Land use greenhouse gas emissions from conventional oil production and oil sands, Environ. Sci. Tech., 44, 8766-8772, http://doi.org/10.1021/es1013278, 2010.

You, Y., Staebler, R. M., Moussa, S. G., Su, Y., Munoz, T., Stroud, C., Zhang, J., and Moran, M. D.: Long-path measurements of pollutants and micrometeorology over Highway 401 in Toronto, Atmos. Chem. Phys., 17, http://doi.org/14119-14143, 10.5194/acp-17-14119-2017, 2017.

https://doi.org/10.5194/amt-2020-116
Preprint. Discussion started: 26 May 2020

Atmospheric Measurement Techniques Discussions

You, Y., Moussa, S. G., Zhang, L., Fu, L., Beck, J., Staebler, R. M.; Determining gas emissions from an oil sands tailings pond with open-path FTIR measurements, In review, Atmos. Chem. Phys., 2020.

Zhang, L., Cho, S., Hashisho, Z., and Brown, C.: Quantification of fugitive emissions from an oil sands tailings pond by eddy covariance, Fuel, 237, 457-464, http://doi.org/10.1016/j.fuel.2018.09.104, 2019.

Zhao, J., Zhang, M., Xiao, W., Wang, W., Zhang, Z., Yu, Z., Xiao, Q., Cao, Z., Xu, J., Zhang, X., Liu, S., and Lee, X.: An evaluation of the flux-gradient and the eddy covariance method to measure CH_4, CO_2, and H_2O fluxes from small ponds, Agric. For. Meterol., 275, 255-264, http://doi.org/10.1016/j.agrformet.2019.05.032, 2019.

https://doi.org/10.5194/amt-2020-116
Preprint. Discussion started: 26 May 2020

Atmospheric Measurement Techniques Discussions

Tables

Table 1 Summary of CH_4 fluxes (g m^{-2} d^{-1}) in this study.

Flux method	Q_25%	median	Q_75%	mean[c]
EC[a]	4.2	5.9	7.9	6.1± 0.5
Gradient[a]	2.6	4.6	7.9	5.7± 1.6
IDM[a]	3.6	5.2	6.6	5.4± 0.4
Flux Chamber[b]	2.0	2.3	3.8	2.8 ±1.4[d]

[a] Statistics and average fluxes are area weight-averaged.

[b] Statistics and average of 15 measurements described in Section 4.6.

[c] Errors with the mean fluxes are calculated with a "top-down" error estimation approach, using the average of standard deviations of fluxes from five periods when the fluxes were relatively steady.

[d] The error is the standard deviation of the 15 measurements. Emission estimates were 5.3 g m^{-2} d^{-1} in 2016 and 11.1 g m^{-2} d^{-1} in 2018.

Table 2 Comparison of CH_4 fluxes (g m^{-2} d^{-1}) in this study to previously reported fluxes.

	TAPOS(2017)	Small et al. (2015)[a]	Stantec report (2016)			Baray et al. (2018)[b]	Flux Chamber 2017
				bubbling zones	quiescent zones		
CH_4	6.1 (EC)	2.6	2013	12.9	2.1	17.1	2.8
			2014	9.6	BDL		
CO_2	18.0 (EC)	16.4	2013	14.9	10.5	NA	21.2
			2014	11.0	BDL		

[a] The original units are tonnes hectare^{-1} year^{-1}. Measurements were taken from August to October in 2010 or 2011. The pond area was 2.8 km^2 as listed in Table 1 of Small et al. (2015). We assumed no seasonal variations to extrapolate from summer measurements to annual totals.

[b]The original number is 2.0 tonnes hour^{-1}, and the pond water surface area was 2.8 km^2 (Small et al, 2015).

https://doi.org/10.5194/amt-2020-116
Preprint. Discussion started: 26 May 2020

Atmospheric Measurement Techniques Discussions

Figures

Figure 1: Map of the study site and the pond in 2017 September.

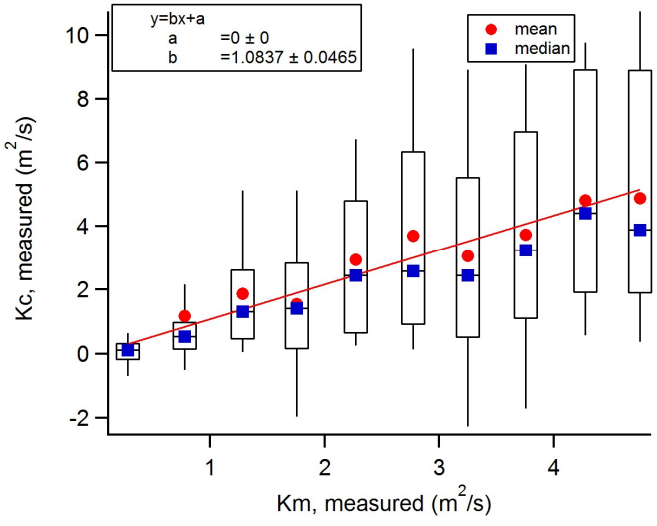

Figure 2: Calculating Schmidt Number S_c as a constant over the entire study.

https://doi.org/10.5194/amt-2020-116
Preprint. Discussion started: 26 May 2020

Atmospheric Measurement Techniques Discussions

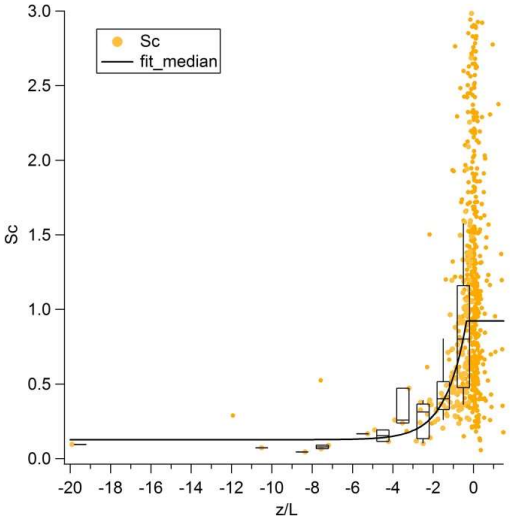

Figure 3: Dependence of S_c on z/L measured at 18m. Yellow points are S_c observed in each individual half-hour period when the wind was from the pond; the black curve is the best fit of S_c verses median z/L from each z/L bin. In this analysis, S_c was binned by z/L with bin width=1 before fitting.

https://doi.org/10.5194/amt-2020-116
Preprint. Discussion started: 26 May 2020

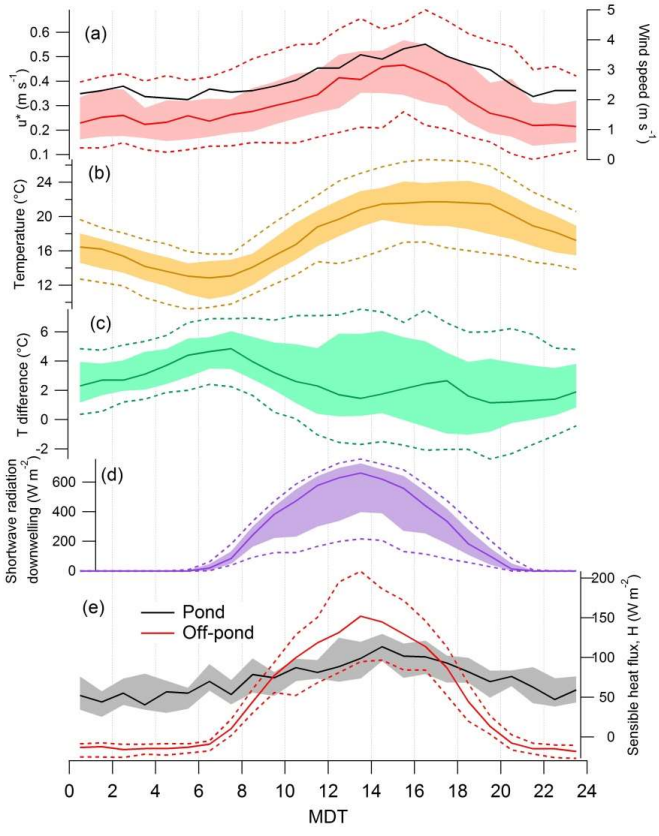

Figure 4: Diurnal variations of (a) u_* at 8m and wind speed at 4m (black); (b) ambient temperature at 8 m; (c) the temperature difference between the surface of the pond and the ambient temperature at 8m; (d) downwelling shortwave radiation; (e) the sensible heat flux at 8m. Solid lines show the median; shades indicate the interquartile ranges; and dashed lines label 10% and 90% percentiles. MDT denotes Mountain Daylight Savings Time (hours).

https://doi.org/10.5194/amt-2020-116
Preprint. Discussion started: 26 May 2020

Atmospheric Measurement Techniques Discussions

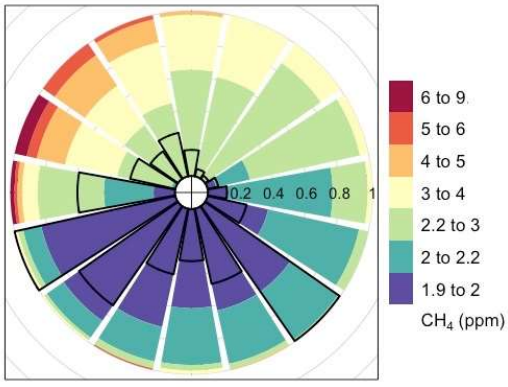

Figure 5: Rose plot of CH_4 mole fraction at 18m. Colors represent CH_4 mole fraction. The length of each colored segment represents the time fraction of that mole fraction range in each direction bin. The radius of the black open sectors indicates the frequency of wind in each direction bin; angle represents wind direction.

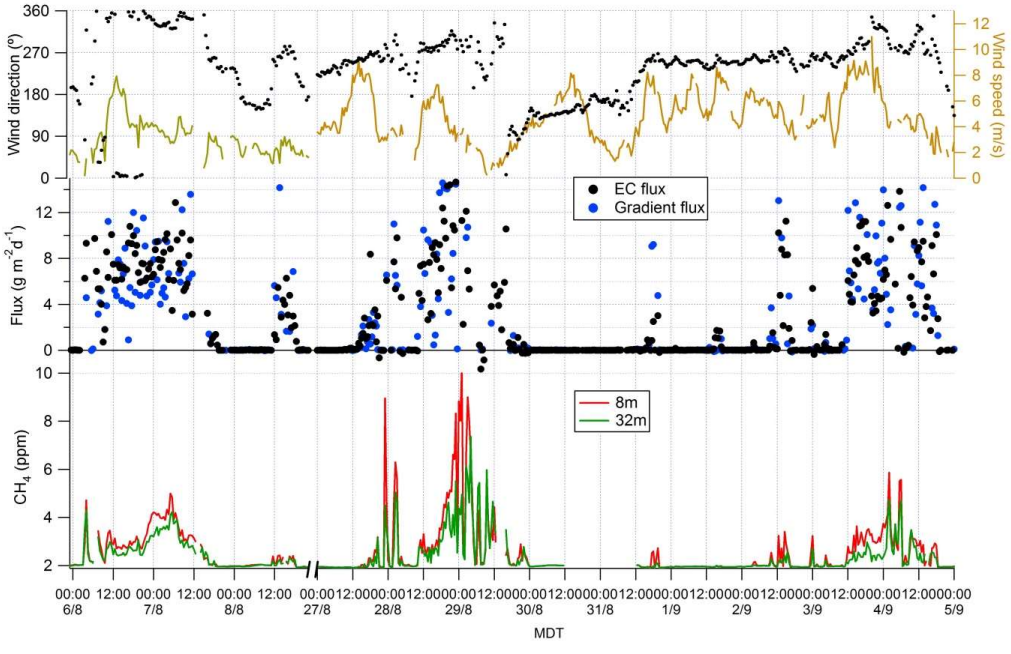

Figure 6: Time series of wind direction, wind speed, CH_4 fluxes, CH_4 mole fraction, from Aug 6th to 9th.

https://doi.org/10.5194/amt-2020-116
Preprint. Discussion started: 26 May 2020

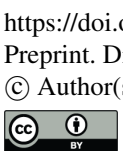

Atmospheric Measurement Techniques Discussions

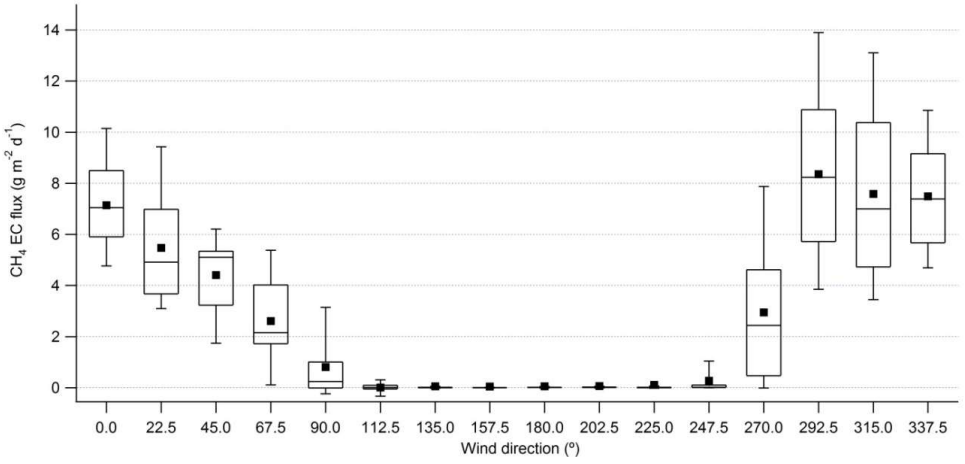

Figure 7: EC flux of CH_4 as a function of wind direction binned in 22.5-degree bins.

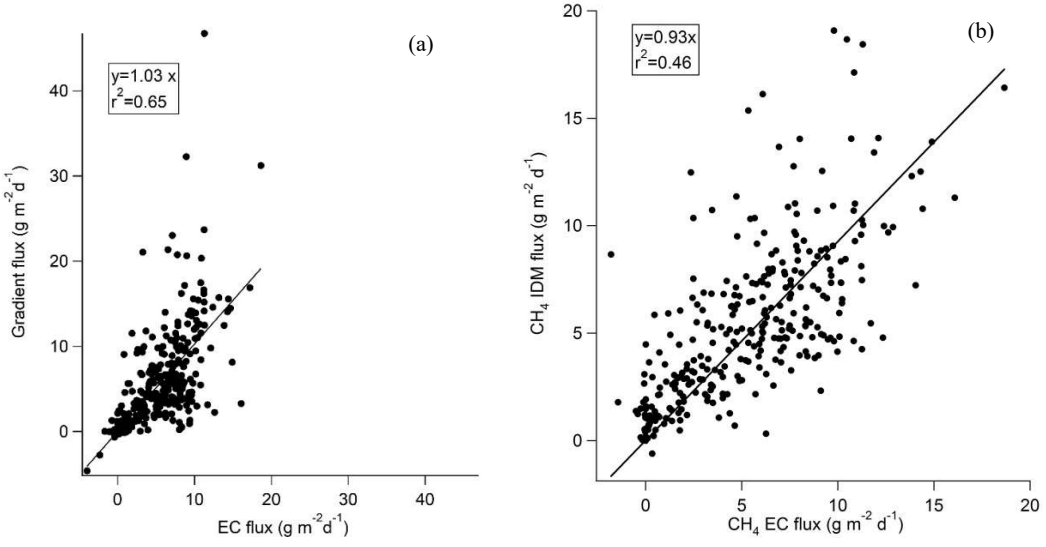

Figure 8: CH_4 gradient flux (a) and IDM flux (b) compared with EC flux.